

Research Paper

Comparison of Plate Vibration and Structural Sound Reduction Using Square-Based Sensor–Actuator Piezoelectric Hybrids with Different Shapes of Sensor Part

Roman TROJANOWSKI *AGH University of Science and Technology
Kraków, Poland*e-mail: roman.cz.trojanowski@agh.edu.pl*Received December 11, 2024; revised June 27, 2025; accepted July 6, 2025;
published online August 20, 2025.*

This work is a continuation of the author's previous research on modeling a piezoelectric sensor–actuator hybrid. It presents the results of vibration and structural sound reduction for a plate with attached piezoelectric elements. The models consist of a steel plate with two piezoelectric actuators attached on one side and a hemispherical air volume on the other side. One of the actuators is used to excite the plate's vibration and has the same shape and size in all models. The second actuator is used for vibration and structural sound reduction and varies between a standard square-based full actuator and a sensor–actuator hybrid with different sizes and shapes of the sensor component (either square- or disc-based). Harmonic analyses were performed for the first four mode shapes (skipping the third mode since it is a square plate). Optimization was performed using internal ANSYS functions, with the objective of minimizing the sum of displacement vectors at a number of nodes corresponding to either the full plate or the sensor placed on the said plate.

Keywords: AVC; FEM; plate vibration; sensors.

Copyright © 2025 The Author(s).
This work is licensed under the Creative Commons Attribution 4.0 International CC BY 4.0
(<https://creativecommons.org/licenses/by/4.0/>).

1. Introduction

During the late 19th century Pierre and Jacques Curie conducted research on various crystals and their properties. They presented their findings in (CURIE, CURIE, 1880), which was the first research paper dealing with the material property now known as piezoelectricity. Today, piezoelectric materials are widely used due to their advantageous properties, such as low power consumption, fast response time and high sensitivity, light weight, flexible sizing, and a wide frequency response range. These materials can be found in microphones, speakers, watches, printers, engines and, of course, in active vibration and sound systems, and more recently, even in energy harvesting applications (MAZUR *et al.*, 2023; WRONA *et al.*, 2022; ISAAC *et al.*, 2022; CHOI *et al.*, 2019). Typically, piezoelectric elements are embedded in or bonded to the surface of a structure to actively control the system's vibration and/or the resulting structural sound (WICIAK,

2008; TROJANOWSKI, WICIAK, 2012). Depending on the piezoelectric effect used, these elements work as actuators or sensors. Piezoelectric materials used for vibration control may consist of single-layer piezoelectric ceramics, multilayer piezoelectric ceramics or composite materials. The foundational work of FULLER *et al.* (1996) and HANSEN and SNYDER (1996) provided much of the necessary theoretical basis for reducing the structural vibrations of simple structures, such as beams and plates using lead zirconate titanate (PZT) elements. Reviews of the modeling of actively controlled piezoelectric smart structures are presented by GUPTA *et al.* (2011) and LI *et al.* (2023).

An important issue regarding the analytical approach to the optimal placement of symmetrical and asymmetrical PZT structures is discussed by BARBONI *et al.* (2000), BRAŃSKI and LIPÍŃSKI (2011), BRAŃSKI (2013), and BRAŃSKI and KURAS (2022). The best results were obtained when the actuator was placed at the point of maximum beam bending moment under

the given boundary conditions. There are also studies that numerically investigated the optimal location of PZT actuators (AUGUSTYN *et al.*, 2014; FAWADE, FAWADE, 2016; KOZIEŃ, ŚCISŁO, 2015). In works by DIMITRIADIS *et al.* (1991), SEKOURI *et al.* (2004), SULLIVAN *et al.* (1996), and WICIAK, TROJANOWSKI (2014b) authors demonstrated the advantages of using distributed actuators of various shapes for active control. Some of the author's previous work focused on materials with step-changing properties (WICIAK, TROJANOWSKI, 2014a). These studies primarily analyzed the efficiency of piezoelectric actuators with different shapes (circular, rectangular, triangular), as well as the effect of step changes in the actuators' material parameters. These analyses showed that even small reductions in vibration levels at particular resonant frequencies could lead to significant changes in the maximum levels of sound pressure radiated by the plate. These reductions in vibration levels were achieved by adjusting the material properties of a particular actuator regions and appropriately increasing the voltage applied to them (WICIAK, TROJANOWSKI, 2015; TROJANOWSKI, WICIAK, 2022). From this research, a new concept emerged: replacing part of the piezoelectric actuator area could create a sensor-actuator hybrid capable of comparable vibration reduction. Numerical models presented in (TROJANOWSKI, WICIAK, 2022) show that such a hybrid is able to achieve similar vibration reduction levels to those of standard (full) actuator, although a higher voltage input is required.

This article is a continuation of the work presented in (TROJANOWSKI, WICIAK, 2022; TROJANOWSKI, 2024), and it presents numerical analyses of a piezoelectric sensor-actuator hybrid composed of a square-based outer section and disc-based inner section. The study includes results of both vibration reduction and sound pressure level reduction.

2. Materials and methods

The object of interest are the vibrations of plates and the resulting sound pressure radiated into the surroundings. For this purpose, a model of a steel plate clamped on all sides, with piezoelectric elements attached to one surface and a hemispherical air domain on the other is considered. Since we continue the previous works (TROJANOWSKI, WICIAK, 2022; TROJANOWSKI, 2024), the dimensions of the modeled objects as well as the material parameters used in models remain the same. Building upon the second iteration of the piezoelectric sensor-actuator hybrid (Figs. 1a, 1b) introduced in (TROJANOWSKI, WICIAK, 2022), this study introduces a modification to the shape of the sensor component (Figs. 1c, 1d).

Changing the shape of the inner part of the sensor-actuator should allow for easier production of physical

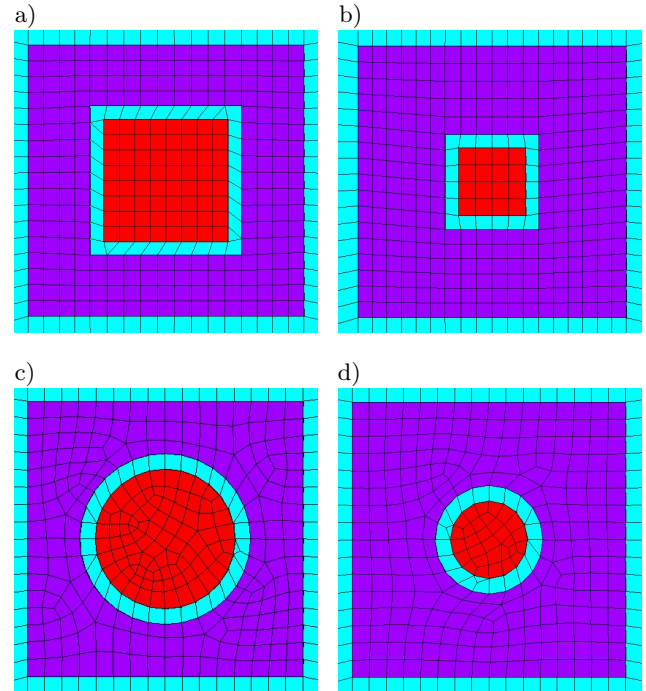


Fig. 1. Concept of a sensor-actuator: a) and b) – square-based sensor-actuators; c) and d) – disc-based sensor-actuators; red – sensor part, violet – actuator part, blue – modeled plate.

prototypes, as eliminating sharp edges makes it easier to cut out parts of piezoelectric elements.

The base of the model is a square steel plate with a side length of 400 mm and a thickness of 2 mm (Fig. 2a). A hemispherical air domain with a radius of 1 m is attached to the plate to simulate the acoustic field near the plate (Fig. 2b). The outer boundary of

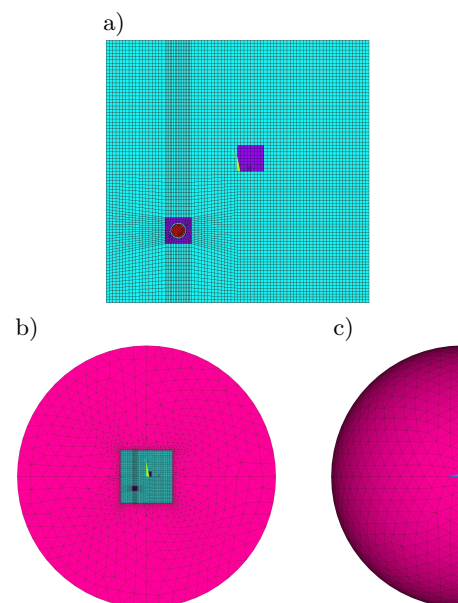


Fig. 2. a) Modeled plate; b) and c) modeled plate with surrounding air.

the air domain is treated as an open space, meaning no reflections occur at the boundary. The vibrations of the plate are excited by a standard square-based piezoelectric actuator placed near the center of the plate. A second piezoelectric element is placed along the diagonal of the plate, approximately $1/4$ of its length, and is used for vibration reduction. Depending on the case, this second element may be a standard square-based piezo actuator or a square-based sensor-actuator hybrid with varying shapes and sizes of the sensor region.

The total base area of the modeled piezoelectric elements is 1600 mm^2 , which corresponds to a side length of 20 mm for the square actuator. All piezoelectric elements have a uniform thickness of 1 mm . In the hybrid configuration, this base area includes the gap between the sensor and actuator parts. The inner sensor part of the hybrid can be either square or disc-shaped and is defined in two sizes:

- for the hybrid with a larger sensor region, the sensor part area ranged from 0 to 0.45 of the side length of the entire element, while the actuator area was from 0.55 to the full side length of the whole element (for a disc-based sensor, this corresponds to 0 to 0.45 of the radius of a disc element with the same base area);
- for the hybrid with a smaller sensor part, the sensor part area ranged from 0 to 0.25 of the radius of the entire element, while the actuator area extended from 0.35 to the full radius of the whole element (for a disc-based sensor, this corresponds to 0 to 0.25 of the radius of a disc element with the same base area).

Table 1 shows the elements and properties used in the model.

Table 1. Parameters used in the model; E – Young’s modulus [Pa]; ν – Poisson’s ratio; ρ – density [kg/m^3]; c – speed of sound in air [m/s].

Structural element	Element in ANSYS library	Properties
Plate	SOLSH190	$E = 1.93 \cdot 10^{11}$ $\nu = 0.29$ $\rho = 7800$
Piezo elements	SOLID226	Properties of PZ28
Air	FLUID30	$\rho = 1.2$ $c = 343$

Harmonic analyses were performed for the 1st, 2nd, 4th, and 5th modes (Fig. 3). It can be seen that the actuator placed near the center of the plate performs very effectively for the 1st and 5th modes. Although the placement is not optimal for the 2nd and especially the 4th mode, it still allows to evaluate the sensor-actuator hybrid under different conditions. The placement of the second actuator/sensor-actuator hybrid was chosen to achieve fairly optimal results across all analyzed modes.

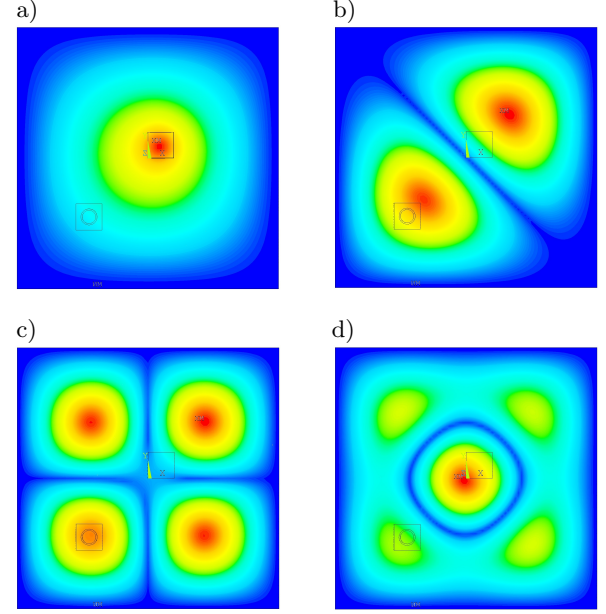


Fig. 3. Analyzed mode shapes: a) 1st (108.6 Hz); b) 2nd (222.1 Hz); c) 4th (330.0 Hz); d) 5th (401.9 Hz).

Figure 4 shows the distribution of sound pressure levels corresponding to the plate’s 1st and 4th mode shapes. The distributions of sound pressure levels are visualized by cutting the hemispherical air domain in half through its center, perpendicular to the plate (in this case, it is cut so we can see the ZY-plane) and then rotating it by 30° . This approach allows visualization of the sound pressure levels above and to the side of the plate.

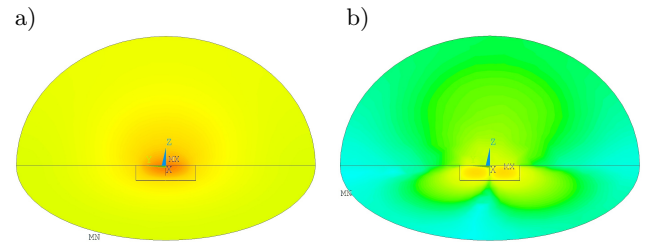


Fig. 4. Examples of sound pressure level distribution before vibration reduction: a) 1st mode; b) 4th mode; reference acoustic pressure is $20 \mu\text{Pa}$.

The voltage applied to the actuators used to excite plates vibrations was 100 V with a phase angle 0° in each case. To find the voltages for vibration reduction, an optimization procedure using ANSYS internal functions was performed. The number of steps for a single run of the optimization procedure was capped at 30 steps. For each run, a voltage range that could be applied to the disc-based element was specified, starting with 0 V – 600 V for the first run. Upon completing the first run of the procedure, another run was initiated using the previous run’s value as the starting point within a narrower voltage range. This process

was repeated until the voltage amplitude range was ± 2.5 V around the starting value.

The phase angle of the voltage applied to the actuator was not treated as a variable for the analyses, as it was shown in previous studies that it should be either 0° or 180° , depending on the mode.

If any of the obtained vibration reduction values differed significantly from the other results, a manual check and tuning were performed.

The goal function used in the optimization procedure is given by

$$J_1 = \min \sum_{i=1}^n |\mathbf{x}_{\text{sum}}(i)|, \quad (1)$$

where min is the minimum value of the sum, $\mathbf{x}_{\text{sum}}(i)$ is the displacement vector sum at the i -th node, n is the total number of nodes considered in the calculation.

Three cases for sensor placement were analyzed, with the possible values of n defined as follows:

- 1) n corresponds to all nodes on the back of the plate (here the back of the plate is the side to which the piezoelectric elements are not attached). The actual number depends on the shape of the hybrid element as well as the ratio between its inner and outer parts (as these parameters influence the finite elements mesh). Typically, this number exceeds 7500 nodes. This is considered the best-case scenario;
- 2) n is equal to 25 nodes forming a ‘virtual’ sensor that covers a quarter of the size of the square-based actuator placed along the same diagonal as the piezoelectric actuators, but on the upper side of the plate (approximately $1/4$ of the plate’s length);
- 3) n is equal to at least 65 nodes forming a ‘virtual’ sensor corresponding in size to the sensor part of the sensor–actuator placed directly beneath it (the exact number changes depending on the sensor part’s size).

3. Results

This section presents the results of the numerical analyses performed. Equation (2) defines how the vibration reduction levels were calculated:

$$L_{\text{red}} = 20 \log_{10} \frac{\sum_{i=1}^n |\mathbf{x}_{1\text{sum}}(i)|}{\sum_{i=1}^n |\mathbf{x}_{2\text{sum}}(i)|}, \quad (2)$$

where $\mathbf{x}_{1\text{sum}}(i)$ is the displacement vector sum at the i -th node before the reduction, $\mathbf{x}_{2\text{sum}}(i)$ is the displacement vector sum at the i -th node after reduction, n is the number of nodes used (corresponding to the three cases mentioned earlier).

Equation (3) shows how the sound pressure level reduction was calculated. For calculations, a slice of the hemispherical air domain with a radius range from 0.4 m to 0.6 m was selected:

$$\text{SPL}_{\text{red}} = 20 \log_{10} \frac{\sum_{j=1}^m |p_1(j)|}{\sum_{j=1}^m |p_2(j)|}, \quad (3)$$

where $p_{1(j)}$ is the sound pressure at the j -th node before reduction, $p_{2(j)}$ is the sound pressure at the j -th node after reduction, m is the number of nodes enclosed within the slice of the hemispherical air domain chosen (depending on the sensor part’s shape and size, at least 992 nodes).

Equation (4) defines how the maximum sound pressure level reduction was calculated:

$$\text{SPL}_{\text{mred}} = \text{SPL}_{\text{max } 1} - \text{SPL}_{\text{max } 2}, \quad (4)$$

where $\text{SPL}_{\text{max } 1}$ is the maximum sound pressure level at any node in the hemispherical air domain before reduction, $\text{SPL}_{\text{max } 2}$ is the maximum sound pressure level in any node of the hemispherical air domain after reduction.

Equation 5 introduces the parameter called voltage efficiency calculated as:

$$UL = \frac{U}{L_{\text{red}}}, \quad (5)$$

where U is the amplitude of voltage applied to the actuator; L_{red} is the level of vibration reduction.

This parameter was introduced as a simplified method to compare the efficiency of different actuator shapes. Since all elements have the same area and are modeled using the same material parameters, this should help to compare the efficiency of piezoelectric elements used in terms of the voltage applied relative to the vibration reduction levels achieved.

Results presented in Tables 2, 3, and 4 showing vibration reduction (columns L_{red} and L_{ref}) as well as voltage efficiency (column UL) for the full actuator, sensor–actuator with larger square sensor and sensor–actuator with smaller square were previously reported in (TROJANOWSKI, WICIAK, 2022). They are presented for comparison reasons and are highlighted with a grey background for clarity.

Table 2 presents the results for vibrations and sound pressure reduction levels achieved when using square-based actuators and sensor–actuators as well as using the entire back area of the plate as a sensor.

The obtained vibration reduction levels for the square-based sensor–actuator with a disc-shaped sensor part range from 26 dB to more than 43 dB. It can be seen that for the 1st mode, all sensor–actuator results are about 0.2 dB–0.3 dB lower than those of the full actuator. Similarly to the findings for the square-based

Table 2. Results obtained for square-based actuators using the entire back area of the plate as a sensor; U_a – amplitude of voltage applied to the actuator; ϕ_a – phase of the voltage applied to the actuator; L_{red} – vibration reduction; UL – voltage efficiency; SPL_{mred} – maximum sound pressure levels reduction; SPL_{red} – overall sound pressure level reduction.

Mode number	Type	U_a [V]	ϕ_a [°]	L_{red} [dB]	UL [V/dB]	SPL_{mred} [dB]	SPL_{red} [dB]
1	Actuator (full)	365.29	180.00	41.3	8.8	41.3	58.1
2		57.77	360.00	43.1	1.3	42.5	40.7
4		12.05	180.00	25.8	0.5	21.5	9.9
5		159.95	360.00	35.0	4.6	33.8	46.1
1	Sensor–actuator (larger square)	558.69	180.00	41.0	13.6	41.4	58.3
2		88.40	360.00	43.1	2.1	42.6	40.4
4		18.38	180.00	26.1	0.7	21.4	9.5
5		247.37	360.00	35.4	7.0	34.2	39.4
1	Sensor–actuator (smaller square)	424.45	180.00	41.0	10.4	41.4	58.7
2		67.14	360.00	43.1	1.6	42.5	40.2
4		14.04	180.00	26.2	0.5	21.4	9.6
5		186.95	360.00	35.4	5.3	34.0	44.4
1	Sensor–actuator (larger disc)	555.11	180.00	41.0	13.6	41.4	58.6
2		87.63	360.00	43.2	2.0	42.6	40.3
4		18.20	180.00	26.0	0.7	21.4	9.9
5		245.09	360.00	35.4	6.9	34.1	44.5
1	Sensor–actuator (smaller disc)	424.81	180.00	41.1	10.3	41.3	58.7
2		66.98	360.00	43.1	1.6	42.6	40.3
4		13.98	180.00	26.0	0.5	21.5	9.9
5		186.29	360.00	35.4	5.3	34.1	44.6

Table 3. Results obtained for square-based actuators when using a ‘virtual’ sensor on the diagonal in the upper side of the plate; L_{redf} – vibration reduction calculated for all nodes on the back side of the plate.

Mode number	Type	U_a [V]	ϕ_a [°]	L_{red} [dB]	L_{redf} [dB]	UL [V/dB]	SPL_{mred} [dB]	SPL_{red} [dB]
1	Actuator (full)	365.42	180.00	44.6	41.3	8.2	41.3	57.8
2		57.80	360.00	53.6	43.0	1.1	42.6	40.7
4		12.20	180.00	23.9	25.9	0.5	21.5	9.9
5		158.66	360.00	31.6	33.7	5.0	33.9	42.8
1	Sensor–actuator (larger square)	558.81	180.00	44.6	41.0	12.5	41.4	58.2
2		88.40	360.00	53.8	43.1	1.6	42.6	40.4
4		18.50	180.00	23.8	25.9	0.8	21.3	9.5
5		247.29	360.00	31.4	35.4	7.9	34.2	44.5
1	Sensor–actuator (smaller square)	424.48	180.00	44.6	41.0	9.5	41.4	58.7
2		67.14	360.00	53.9	43.1	1.2	42.5	40.2
4		14.04	180.00	23.8	26.2	0.6	21.4	9.6
5		186.81	360.00	31.5	35.4	5.9	34.1	44.4
1	Sensor–actuator (larger disc)	555.05	180.00	44.6	41.0	12.5	41.4	58.6
2		87.62	360.00	54.0	43.2	1.6	42.6	40.3
4		18.24	180.00	23.8	26.0	0.8	21.4	10.0
5		245.03	360.00	31.4	35.4	7.8	34.1	44.5
1	Sensor–actuator (smaller disc)	424.82	180.00	44.6	41.1	9.5	41.3	58.7
2		66.98	360.00	54.0	43.1	1.2	42.6	40.3
4		14.04	180.00	23.8	26.0	0.6	21.5	9.9
5		186.46	360.00	31.5	35.4	5.9	33.9	44.5

sensor part (TROJANOWSKI, WICIAK, 2022), there seems to be virtually no difference for the 2nd mode. For the 4th mode, all the sensor–actuators achieve vibration reduction levels around 0.2 dB–0.3 dB higher than the standard actuators, and this difference rises to about 0.4 dB for the last analyzed mode. None of these differences can be called significant, and there is almost no variation in vibration reduction level results when comparing hybrids with different sensor shapes and sizes.

As for the voltages applied to the sensor–actuator, since changes in the sensor part shape do not significantly change the required voltages, the findings presented in (TROJANOWSKI, WICIAK, 2022) are still valid. The full actuator requires less voltage to achieve the results shown, but reducing the sensor part size can somewhat mitigate this difference.

Table 3 presents the results of vibration and acoustic pressure levels reduction for square-based actuators and sensor–actuators in the scenario where the sensor

Table 4. Results obtained for square-based actuators using a ‘virtual’ sensor placed beneath the center of the square-based actuator.

Mode number	Type	U_a [V]	ϕ_a [°]	L_{red} [dB]	L_{redf} [dB]	UL [V/dB]	SPL_{mred} [dB]	SPL_{red} [dB]
1	Actuator (full)	363.40	180.00	25.4	39.2	14.3	40.7	45.1
2		57.76	360.00	41.9	43.1	1.4	42.5	40.7
4		12.27	180.00	31.4	25.7	0.4	21.4	10.0
5		161.03	360.00	33.4	34.4	4.8	32.1	40.3
1	Sensor–actuator (larger square)	557.24	180.00	26.0	40.2	21.4	41.2	50.5
2		88.45	360.00	42.8	43.1	2.1	42.6	40.4
4		18.36	180.00	32.2	26.1	0.6	21.4	9.5
5		247.48	360.00	35.1	35.4	7.1	34.2	44.5
1	Sensor–actuator (smaller square)	423.19	180.00	25.5	40.0	16.6	41.1	49.6
2		67.14	360.00	42.2	43.1	1.6	42.5	40.2
4		14.05	180.00	32.0	26.1	0.4	21.4	9.6
5		186.85	360.00	34.0	35.4	5.5	34.1	44.4
1	Sensor–actuator (larger disc)	553.37	180.00	26.0	40.0	21.3	41.1	49.5
2		87.64	360.00	42.8	43.2	2.0	42.6	40.3
4		18.21	180.00	32.3	26.0	0.6	21.4	9.9
5		245.01	360.00	35.0	35.4	7.0	34.1	44.5
1	Sensor–actuator (smaller disc)	423.48	180.00	25.5	40.1	16.6	41.0	49.0
2		66.98	360.00	42.1	43.1	1.6	42.6	40.3
4		13.98	180.00	32.0	26.0	0.4	21.5	9.9
5		186.08	360.00	33.9	35.4	5.5	34.2	44.5

is placed on the same diagonal as the actuator used for reduction, but located in the upper right quarter of the plate.

In this scenario, vibration reduction levels obtained range from nearly 24 dB (23.8 dB) for the 4th mode to 54 dB for the 2nd mode, regardless of the shape of the sensor part of the sensor–actuator hybrid. The largest difference between the full actuator and a sensor–actuator hybrid with a disc-shaped sensor part occurs in the 2nd mode and is about 0.4 dB, regardless the size of the sensor part of the hybrid. Again, there is almost no difference in performance among sensor–actuators, regardless of the size or shape of the sensor part.

As for the voltage efficiency, the same trend observed in (TROJANOWSKI, WICIAK, 2022) and in Table 2 is clearly apparent here. Using sensor–actuator hybrid results in higher values of UL . While changing the shape of the sensor part in the sensor–actuator hybrid does change the voltages that have to be applied to achieve vibration reduction, these changes are minor. Full actuators require less voltage to achieve similar vibration reduction levels due to their larger active area.

Table 4 presents the results for vibration and acoustic pressure levels reduction when using square-based actuators in a scenario where the sensor is placed beneath the center of the actuator (or sensor–actuator) and matches the size of the sensor part of the sensor–actuator.

In this scenario, vibration reduction levels for the disc-based hybrids range from around 25.5 dB for the 1st mode to almost 43 dB for the 2nd mode. For

this sensor placement, the sensor–actuator hybrids achieve slightly higher vibration reduction levels in every case (up to 1.6 dB). Again, changing the shape of the sensor part does not significantly influence the results.

As for the UL values, we can observe a similar trend to that observed in data in Tables 2 and 3. While the values differ depending on the vibration reduction levels achieved, the ratios between different actuator types are similar to those observed in previous cases.

Similarly as in (TROJANOWSKI, WICIAK, 2022; TROJANOWSKI, 2024), the next step in presenting the results is recalculating the vibration reduction levels for the best-case scenario – using the back of the plate as the sensor (L_{redf} column in Tables 3 and 4, and L_{red} column in Table 2). These results are shown in Fig. 5.

The first five bars for each mode represent the results from the first case (Table 2, discussed earlier).

The middle five bars for each mode show the results for the sensor placed on the diagonal, about one-quarter of the plate’s length from the upper right side, recalculated to match the results for the full plate sensor scenario. It can be seen that these results are very similar to those of the first case. For the 1st mode, vibration reduction levels achieved using the sensor–actuator hybrids are about 0.2 dB–0.3 dB lower than those of the full actuator. There are almost no differences observed in the results for the 2nd mode. For the 4th mode, standard actuators achieve slightly lower reduction levels (up to 0.4 dB less). The biggest differences can be observed in the vibration reduction levels for the 5th mode. In this mode, sensor–actuator hybrids achieved results higher than those of the stan-

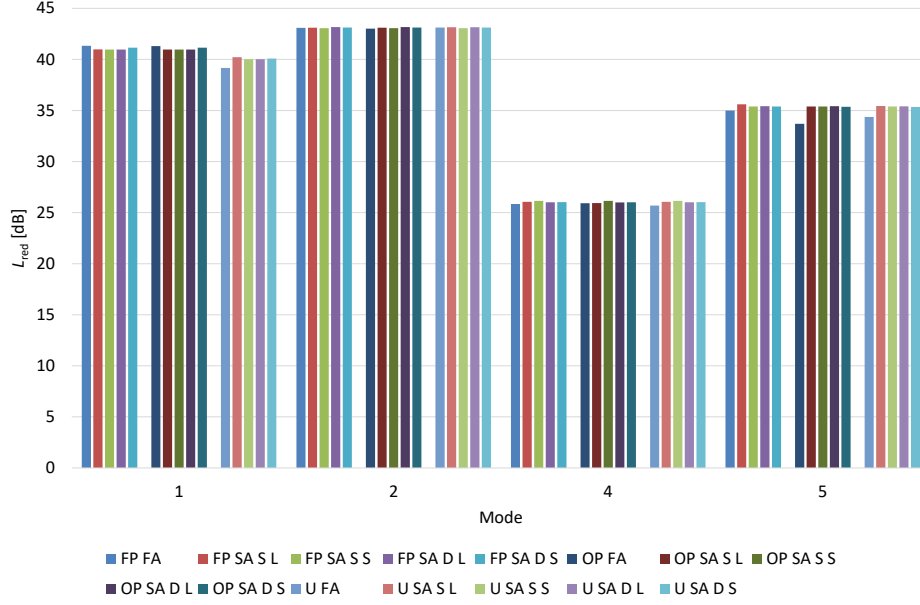


Fig. 5. Comparison of vibration reduction levels obtained for square-based actuators, recalculated for the full plate; FP – scenario using the whole back of the plate as a sensor; OP – sensor placed on the diagonal in the upper right quadrant of the plate; UP – sensor placed beneath the actuator (or sensor-actuator); FA – full actuator; SA S L – sensor-actuator with larger square-based sensor part; SA S S – sensor-actuator with smaller square-based sensor part, SA D L – sensor-actuator with larger disc-based sensor part; SA D S – sensor-actuator with smaller disc-based sensor part.

dard actuator by 1.7 dB. Differences between the recalculated results for the piezoelectric hybrid elements do not exceed 0.3 dB.

The last five bars represent the recalculated results for the scenario where the sensor corresponding in size and placement to the sensor part of the sensor-actuator. For the 1st mode, it can be seen that vibration reduction levels for this case are lower than in the other two scenarios – about 2.1 dB lower for the full actuator and 0.8 dB–1.0 dB lower for the sensor-actuator hybrids. This translates to the full actuator showing approximately 0.8 dB to 1.0 dB lower vibration reduction than the sensor-actuator hybrids in this scenario. For the 2nd and 4th modes, the obtained results are similar to those of the other two cases. For the 5th mode, it can be seen that results obtained for the sensor-actuator hybrids are higher by about 1.0 dB than the results for the full actuator. The differences in vibration reduction levels between the full actuators and sensor-actuator hybrids for the 1st and 5th modes in this scenario can be attributed to the presence of the ‘working’ part of the actuator occupying the same place as the sensor in the full actuator case. However, since this situation does not occur for the 2nd and 4th mode, and if we take into account the mode shapes shown in Figs. 2a and 3, it can be assumed that the actuator placement relative to the mode shapes impacts these differences.

The differences between different shapes and sizes of the sensor part of the sensor-actuator hybrids do not exceed 0.2 dB.

In (TROJANOWSKI, WICIAK, 2022), it was proposed that reducing the size of the sensor part in a sensor-actuator hybrid does not influence the vibration reduction levels obtained when using said hybrids. This observation seems to hold true even after changing the shape of the sensor part. Based on the results presented in this paper, we can add another assumption that changing the sensor part of a square-based sensor-actuator hybrid from square to disc-shaped also does not have a significant impact on the results of vibration reduction levels obtained. This is a positive finding, as it should be easier to produce physical prototypes of hybrids with a disc-shaped sensor part than with a square-shaped one.

The final step in presenting the results focuses on the acoustic pressure level reductions accompanying vibration reduction of the plates. These results are presented in Tables 2, 3, and 4 as well as in Fig. 6.

The leftmost five bars for each mode represent the sound pressure reduction when using the whole back area of the plate as a sensor. The obtained sound pressure reductions range from about 9.5 dB for the 4th mode up to almost 59 dB for the 1st mode. It can be seen that for the 1st mode, higher values of sound pressure reduction are obtained for the sensor-actuator hybrids than for the full actuator, despite the full actuator achieving about 0.3 dB greater vibration reduction. Although these differences are not significant (at most, around 0.6 dB), they occur across all hybrid configurations. For the 2nd and 4th modes, the differences in sound pressure level reduction among the modeled

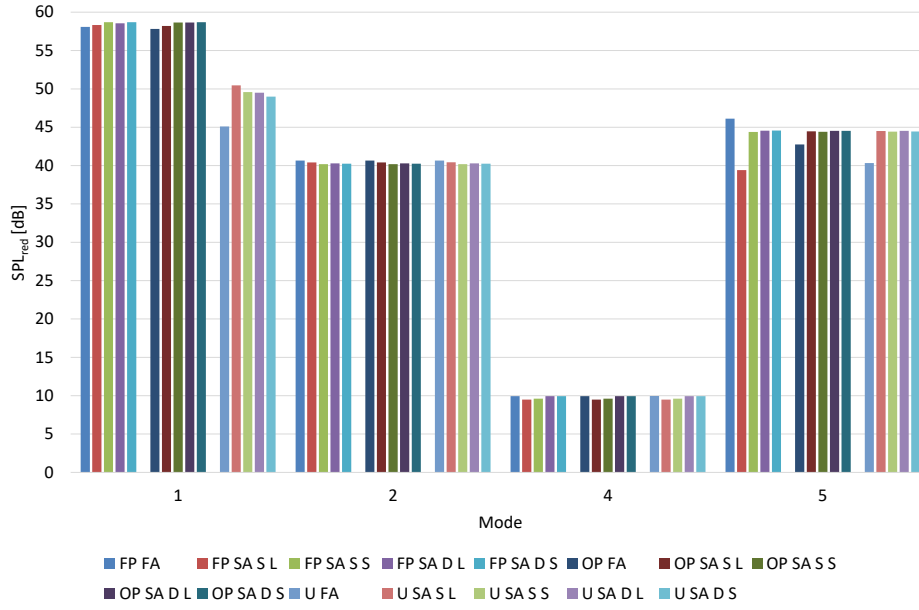


Fig. 6. Comparison of acoustic pressure levels reductions obtained for square-based actuators.

actuators are no greater than 0.5 dB. However, for the 5th mode, there are two interesting observations. First, the full actuator achieves the highest sound pressure level reduction, around 1.6 dB greater than most of the sensor-actuator hybrids. Second, the hybrid with the larger square-based sensor part achieves significantly lower sound pressure level reduction (around 5 dB) than the other hybrids, and around 6.7 dB less than the full actuator. This occurs at the same time when the vibration reduction levels corresponding to that sound pressure level reduction are the highest among all modeled actuators/sensor-actuator hybrids. This, coupled with the vibration reduction level data (Fig. 5), sound pressure level reduction results for other sensor placements and sizes (Fig. 6), the maximum sound pressure level reduction and the small differences in voltages applied to actuators to achieve these results (Tables 2–4), may indicate that this anomaly is the results of a specific vibration distribution pattern of the plate.

The middle five bars for each mode represent the sound pressure reduction accompanying the plate's vibration reduction when using a sensor placed on the diagonal opposite the actuator placement. It can be seen that for the 1st, 2nd, and 4th modes, these results are very similar to the results obtained from the previous scenario. The biggest difference can be seen in the 5th mode. In this scenario, all sensor-actuator hybrids achieve very similar values of sound pressure level reduction (with no anomaly as observed in the previous case) and these reductions are about 1.7 dB higher than those achieved using a full actuator.

The five bars on the right, for each mode, represent the sound pressure reduction accompanying the plate's vibration reduction when using a sensor corre-

sponding in size and placement to the sensor part of the sensor-actuator. Here, the sound pressure level reduction ranged from 9.5 dB for the 4th mode to 50.5 dB for the 1st mode. For the 1st mode, the small decrease in overall vibration level reduction obtained compared to previous scenarios (about 2.1 dB for the full actuator and 0.8 dB–1.0 dB for the sensor-actuators) results in a significant reduction in corresponding sound pressure level reduction (around 13 dB for the full actuator and around 8 dB–10 dB for the sensor actuator hybrids). For the 2nd and 4th modes, again, there are no significant changes in results. In the 5th mode, the sound pressure level reduction achieved using the full actuator was more than 4 dB lower than the one obtained using sensor-actuator hybrids.

It can be seen that changing the shape or size of the sensor part of the sensor-actuator hybrid does not have a significant impact on the sound pressure level reduction results.

Figure 7 shows examples of sound pressure level distributions before (left column) and after (right column) the plate's vibration reduction. The presented figure is for the first scenario (using full back area of the plate as a sensor) and compares the full actuator with a square-based sensor-actuator and a larger disc-based sensor part. It can be observed that the change in SPL_{red} values are not solely due to a decrease in sound pressure levels radiating from the plate, but also due to a change in the type of sound source that the plate represents. For example, in the 1st mode, before vibration reduction, the plate acts like a monopole sound source, while after reduction it behaves like a dipole. Similar changes can be seen in the 4th and 5th modes, where the sound pressure distribution also shift following the plate's vibration reduction. In a way, the pattern flips –

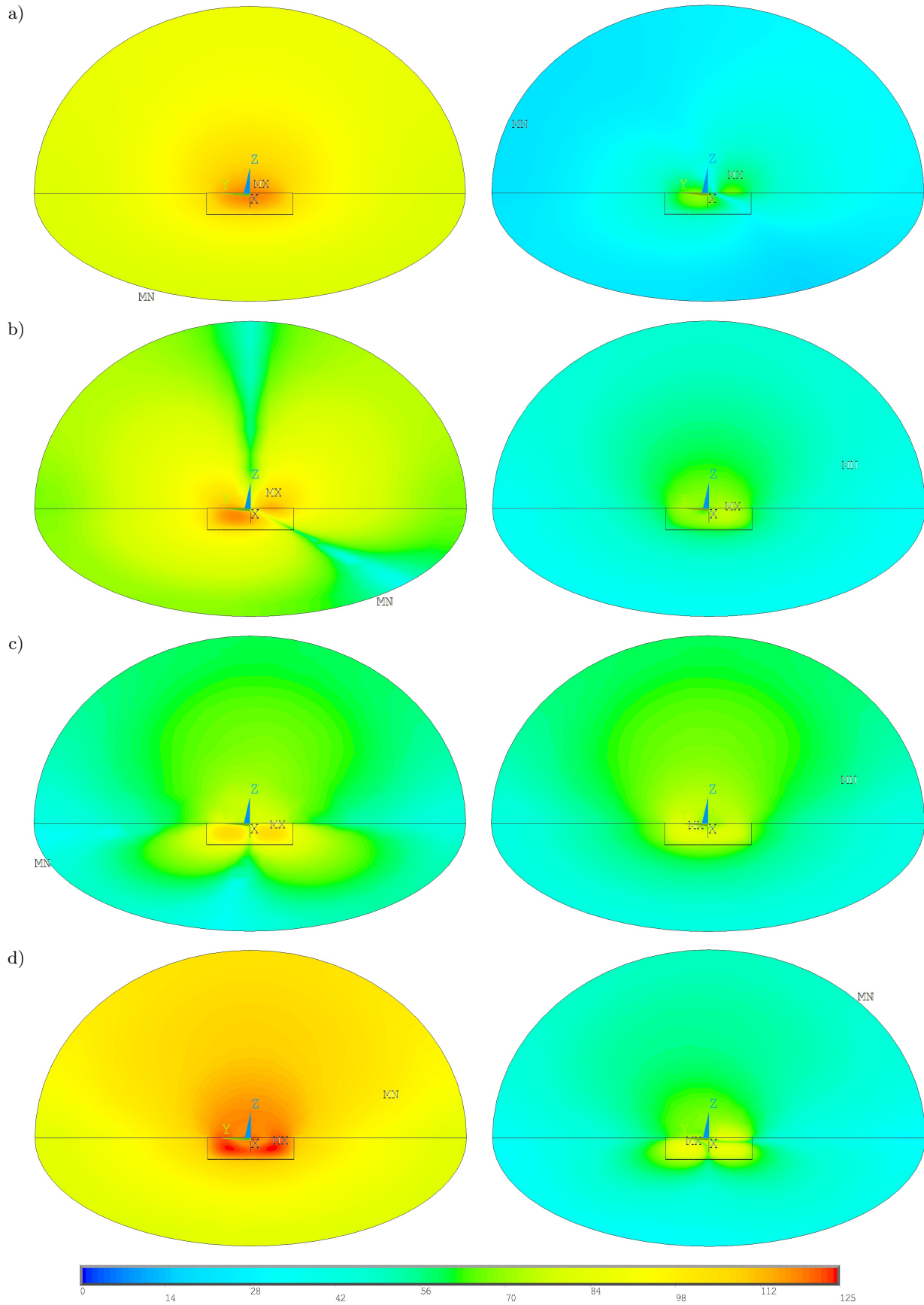


Fig. 7. Examples of sound pressure level distributions before (left column) and after (right column) plate vibration reduction for different modes: a) 1st mode; b) 2nd mode; c) 4th mode; d) 5th mode; reference acoustic pressure: 20 μPa .

for the 4th mode, the plate's vibration pattern initially resembles a quadrupole and transitions to a 'ring-like' pattern (with a sound pressure distribution similar to that of a monopole) after reduction. Conversely, in the 5th mode, this situation is reversed – it begins with a 'ring-like' pattern and transitions to a quadrupole. This change is partially responsible for the difference observed between SPL_{mred} (reduction of the maximum sound pressure levels) and SPL_{red} (reduction of sound pressure levels in a portion of the hemispherical volume) values, as shown in Tables 2–4. For example, in the 4th mode, SPL_{mred} exceeds 21 dB for every type of actuator, while SPL_{red} remains below 10 dB.

4. Conclusions

For the analyzed modes, changing the shape of the sensor part in a square-based sensor–actuator hybrid does not seem to significantly change its performance. The proposed square-based hybrid with a disc-shaped sensor part appears to be capable of achieving vibration reduction levels comparable to those of a standard actuator. In some cases, the results obtained for the hybrid were slightly higher than those for the full actuator, although the differences were not really significant. The sensor part appears to function effectively, and the results are fairly comparable in every scenario.

Similarly, square-based sensor–actuator hybrids demonstrate sound pressure level reductions comparable to those achieved by full actuators when taking into account sound vibration in the plate reduction. The downside of using sensor–actuators is the higher voltage required to achieve vibration reduction levels comparable to those of standard actuators. This is expected, as the actuator part of the sensor–actuator is smaller than a full actuator. Also, this can be partially mitigated by using a smaller sensor part.

The next step of this research will involve creating a physical prototype of the sensor–actuator based on the second iteration models, followed by physical experiment to confirm the numerical results. As for numerical modeling, next we will determine the optimal ratios between the sensor and actuator parts.

FUNDING

The work described in this paper has been executed within the statutory activities of the Faculty of Mechanical Engineering and Robotics of AGH – University of Science and Technology (No. 16.16.130.942).

CONFLICT OF INTEREST

The author declare that he has no known competing financial interests or personal relationships that could have appeared to influence the work reported in this paper.

References

1. AUGUSTYN E., KOZIEŃ M.S., PRAĆIK M. (2014), FEM analysis of active reduction of torsional vibrations of clamped-free beam by piezoelectric elements for separated mode, *Archives of Acoustics*, **39**(4): 639–644, <https://doi.org/10.2478/aoa-2014-0069>.
2. BARBONI R., MANNINI A., FANTINI E., GAUDENZI P. (2000), Optimal placement of PZT actuators for the control of beam dynamics, *Smart Materials and Structures*, **9**: 110–120, <https://doi.org/10.1088/0964-1726/9/1/312>.
3. BRAŃSKI A. (2013), Effectiveness analysis of the beam modes active vibration protection with different number of actuators, *Acta Physica Polonica A*, **123**(6): 1123–1127, <https://doi.org/10.12693/APhysPolA.123.1123>.
4. BRAŃSKI A., KURAS R. (2022), Asymmetrical PZT applied to active reduction of asymmetrically vibrating beam – Semi-analytical solution, *Archives of Acoustics*, **47**(4): 555–564, <https://doi.org/10.24425/aoa.2022.142891>.
5. BRAŃSKI A., LIPÍŃSKI G. (2011), Analytical determination of the PZTs distribution in active beam vibration protection problem, *Acta Physica Polonica A*, **119**(6A): 936–941.
6. CHOI J., JUNG I., KANG Ch.-Y. (2019), A brief review of sound energy harvesting, *Nano Energy*, **56**: 169–183, <https://doi.org/10.1016/j.nanoen.2018.11.036>.
7. CURIE J., CURIE P. (1880), Development, via compression, of electric polarization in hemihedral crystals with inclined faces [in French], *Bulletin de la Societe de Minerologie de France*, **3**: 90–93, <https://doi.org/10.3406/bulmi.1880.1564>.
8. DIMITRIADIS E.K., FULLER C.R., ROGERS C.A. (1991), Piezoelectric actuators for distributed vibration excitation of thin plates, *Journal of Vibration and Acoustics*, **113**: 100–107, <https://doi.org/10.1115/1.2930143>.
9. FAWADE A.S., FAWADE S.S. (2016), Modeling and analysis of vibration controlled cantilever beam bounded by PZT patch, *International Journal of Engineering Inventions*, **5**(7): 7–14.
10. FULLER C.R., ELLIOTT S.J., NELSON P.A. (1996), *Active Control of Vibration*, Academic Press, London.
11. GUPTA V., SHARMA M., THAKUR N. (2011), Mathematical modelling of actively controlled piezo smart structures: A review, *Smart Structures and Systems*, **8**(3): 275–302, <https://doi.org/10.12989/sss.2011.8.3.275>.
12. HANSEN C.H., SNYDER S.D. (1996), *Active Control of Noise and Vibration*, CRC Press, London, <https://doi.org/10.1201/9780367804831>.
13. ISAAC C.W., WRONA S., PAWEŁCZYK M., KARIMI H.R. (2022), Modelling vibro-acoustic response of lightweight square aluminium panel influenced by sound source locations for active control, *Scientific Reports*, **12**(1): 10727, <https://doi.org/10.1038/s41598-022-14951-y>.

14. KOZIEŃ M.S., ŚCISŁO Ł. (2015), Simulation of control algorithm for active reduction of transversal vibrations of beams by piezoelectric elements based on identification of bending moment, *Acta Physica Polonica A*, **128**(1A): 56–61, <https://doi.org/10.12693/APhysPolA.128.A-56>.
15. LI J., ZHANG L., LI S., MAO Q., MAO Y. (2023), Active disturbance rejection control for piezoelectric smart structures: A review, *Machines*, **11**(2): 174, <https://doi.org/10.3390/machines11020174>.
16. MAZUR K., PAWEŁCZYK M., KARIMI H.R. (2023), Global noise reduction in free-field conditions by using active noise-controlling casings, *Mechanical Systems and Signal Processing*, **197**: 110393, <https://doi.org/10.1016/j.ymssp.2023.110393>.
17. SEKOURI E.M., HU Y.R., NGO A.D. (2004), Modelling of a circular plate with piezoelectric actuators, *Mechatronics*, **14**(9): 1007–1020, <https://doi.org/10.1016/j.mechatronics.2004.04.003>.
18. SULLIVAN J.M., HUBBARD J.E. Jr., BURKE S.E. (1996), Modeling approach for two-dimensional distributed transducers of arbitrary spatial distribution, *The Journal of the Acoustical Society of America*, **99**(5): 2965–2974, <https://doi.org/10.1121/1.414861>.
19. TROJANOWSKI R. (2024), Piezoelectric disc based sensor-actuator hybrid in vibration reduction, *Vibrations in Physical Systems*, **35**(1): 2024117-1–2024117-9, <https://doi.org/10.21008/j.0860-6897.2024.1.17>.
20. TROJANOWSKI R., WICIAK J. (2012), Structural noise reduction and its effects on plate vibrations, *Acta Physica Polonica A*, **121**(1A): A-148–A-151, <https://doi.org/10.12693/APhysPolA.121.A-148>.
21. TROJANOWSKI R., WICIAK J. (2020), Impact of the size of the sensor part on sensor-actuator efficiency, *Journal of Theoretical and Applied Mechanics*, **58**(2): 391–401, <https://doi.org/10.15632/jtam-pl/118948>.
22. TROJANOWSKI R., WICIAK J. (2022), Piezoelectric square based sensor-actuator hybrid in vibration reduction, *Vibrations in Physical Systems*, **33**(3): 2022303-1–2022303-9, <https://doi.org/10.21008/j.0860-6897.2022.3.03>.
23. WICIAK J. (2008), Sound radiation by set of L-jointed plates with four pairs of piezoelectric elements, *The European Physical Journal Special Topics*, **154**: 229–233, <https://doi.org/10.1140/epjst/e2008-00551-0>.
24. WICIAK J., TROJANOWSKI R. (2014a), The effect of material composition of piezoelectric elements with chosen shapes on plate vibration reduction, *Acta Physica Polonica A*, **125**(4A): A-179–A-182, <https://doi.org/10.12693/APhysPolA.125.A-179>.
25. WICIAK J., TROJANOWSKI R. (2015), Evaluation of the effect of a step change in piezo actuator structure on vibration reduction level in plates, *Archives of Acoustics*, **40**(1): 71–79, <https://doi.org/10.1515/aoa-2015-0009>.
26. WICIAK M., TROJANOWSKI R. (2014b), Numerical analysis of the effectiveness of two-part piezoactuators in vibration reduction of plates, *Acta Physica Polonica A*, **125**(4A): A-183–A-189, <https://doi.org/10.12693/APhysPolA.125.A-183>.
27. WRONA S., PAWEŁCZYK M., CHENG L. (2022), Sound transmission through a panel with a hybrid active and semi-active control system, *Journal of Sound and Vibration*, **536**: 117172, <https://doi.org/10.1016/j.jsv.2022.117172>.